

INFRARED PROPERTIES OF OGLE4 MIRA VARIABLES IN OUR GALAXY

KYUNG-WON SUH

Department of Astronomy and Space Science, Chungbuk National University, Chungbuk, Cheongju-City 28644, Korea;
 kwsuh@chungbuk.ac.kr

Received September 16, 2022; accepted November 22, 2022

Abstract: We investigate infrared properties of OGLE4 Mira variables in our Galaxy. For each object, we cross-identify the AllWISE, 2MASS, Gaia, and IRAS counterparts. We present various IR two-color diagrams (2CDs) and period-magnitude and period-color relations for the Mira variables. Generally, the Mira variables with longer periods are brighter in the IR fluxes and redder in the IR colors. In this work, we also revise and update the previous catalog of AGB stars in our Galaxy using the new sample of OGLE4 Mira variables. Now, we present a new catalog of 74,093 (64,609 O-rich and 9484 C-rich) AGB stars in our Galaxy. A group of 23,314 (19,196 O-rich and 4118 C-rich) AGB stars are identified based on the IRAS PSC and another group of 50,779 (45,413 O-rich and 5366 C-rich) AGB stars are identified based on the AllWISE source catalog. For all of the AGB stars, we cross-identify the IRAS, AKARI, MSX, AllWISE, 2MASS, OGLE4, Gaia, and AAVSO counterparts and present various infrared 2CDs. Comparing the observations with the theory, we find that basic theoretical dust shell models can account for the IR observations fairly well for most of the AGB stars.

Key words: Long Period Variables — stars: AGB and post-AGB — circumstellar matter — infrared: stars — radiative transfer

1. INTRODUCTION

Most asymptotic giant branch (AGB) stars are believed to be long-period variables (LPVs) with outer dust envelopes (e.g., [Suh 2021](#)). LPVs are classified into small-amplitude red giants (SARGs), semiregular variables (SRVs), and Mira variables (e.g., [Soszyński et al. 2013](#)). Though most of SRVs and a majority of SARGs could also be in the AGB phase, all Mira variables are known to be in the AGB phase (e.g., [Höfner & Olofsson 2018](#)).

Depending on the chemical composition of the photosphere or the outer dust envelope, AGB stars are classified into O-rich or C-rich stars. Amorphous silicates in the envelopes around O-rich AGB (OAGB) stars produce 10 μm and 18 μm features in emission or absorption (e.g., [Suh 1999](#)). Dust envelopes around C-rich AGB (CAGB) stars consist of amorphous carbon (AMC) and SiC dust (e.g., [Suh 2000](#)). SiC dust produces the 11.3 μm emission feature.

[Suh \(2021\)](#) presented a catalog of 11,209 OAGB stars and 7172 CAGB stars in our Galaxy and presented various IR two-color diagrams (2CDs) for the AGB stars. The IR 2CDs have been useful in studying the chemical and physical properties of various celestial objects (e.g., [van der Veen & Habing 1988](#); [Suh 2015](#)).

Thanks to the optical gravitational lensing experiment IV (OGLE4) project, the number of known Mira variable in our Galaxy has increased significantly. [Iwanek et al. \(2022\)](#) presented a sample of 65,981 OGLE4 Mira variables in our Galaxy, from which the majority (47,532 objects) comprises new discoveries.

In this work, we investigate IR properties of

OGLE4 Mira variables in our Galaxy. For each object, we cross-identify the Wide-field Infrared Survey Explorer (WISE), Two-Micron All-Sky Survey (2MASS), and Infrared Astronomical Satellite (IRAS) counterparts. We present period-magnitude and period-color relations for the Mira variables. We also revise and update the previous catalog of AGB stars in our Galaxy using the new sample of OGLE4 Mira variables. For the new list of AGB stars, we cross-identify the IRAS, AKARI, Midcourse Space Experiment (MSX), AllWISE, 2MASS, OGLE4, Gaia Data Release 3 (DR3), and American Association of Variable Star Observers (AAVSO; international variable star index; version 2022 September 23; [Watson et al. 2022](#)) counterparts and present various IR 2CDs. We compare the observations with theoretical models and discuss general properties of the AGB stars.

2. OGLE4 MIRA VARIABLES IN OUR GALAXY

[Iwanek et al. \(2022\)](#) presented a sample of 65,981 OGLE4 Mira variables in our Galaxy (40,356 objects in the Galactic bulge fields and 25,625 objects in the Galactic disk).

2.1. Infrared Photometric Data

The IRAS point source catalog (PSC) ([Beichman et al. 1988](#)) provided photometric data at four bands (12, 25, 60, and 100 μm) for 245,889 objects. The IRAS's photometric sensitivity (averaged 10 sigma value at the 12 μm band) is 0.7 Jy. MSX ([Egan et al. 2003](#)) conducted the Galactic plane survey with a higher sensitivity (about 0.17 Jy at the 8.28 μm band) at four MIR bands (8.28, 12.13, 14.65, and 21.34 μm) for 454,091

Table 1
OGLE4 Mira variables in our Galaxy

OGLE4M ¹	AllWISE ²	2MASS ²	Gaia ^{2,3}	IRAS ⁴
65,981	64,962	65,931	57,482	16,379

¹OGLE4 Mira variables from Iwanek et al. (2022). ²The number of counterparts within 5'' (2'' for Gaia; duplicate sources are excluded). ³ Gaia DR3 LPV sources (Lebzelter et al. 2022). ⁴The number of positive counterparts of IRAS PSC sources within 60'' (see Section 2.7).

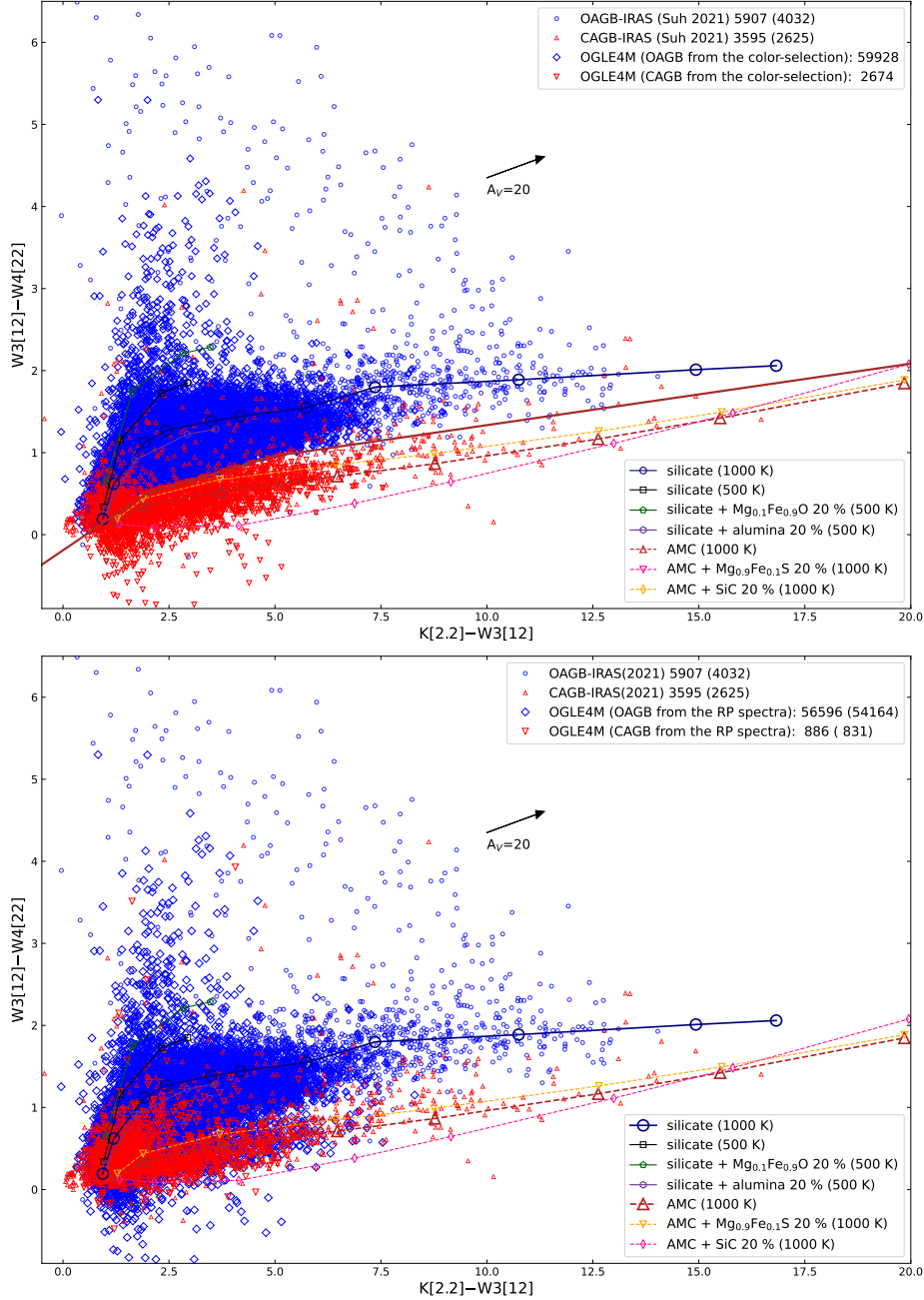


Figure 1. WISE-2MASS 2CDs for color-selected OAGB and CAGB stars (the upper panel; see Section 2.4) and for OAGB and CAGB stars classified from the Gaia RP spectra (the lower panel; see Section 2.5) for the OGLE4 Mira variables. The 2CDs also show known AGB stars from Suh (2021) (see Table 3). The observations are compared with theoretical models (see Section 4.1). The brown line in the upper-panel shows the boundary line between OAGB and CAGB stars for the color-selection method. The number of objects and the number of plotted objects (in parenthesis) with good-quality observed data are shown for each class.

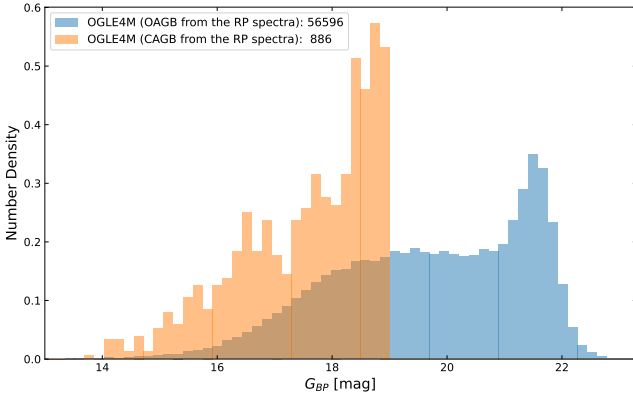


Figure 2. Number density distributions of the Gaia magnitudes at the BP band for OAGB and CAGB stars classified from the Gaia RP spectra for the OGLE4 Mira variables (see Section 2.5).

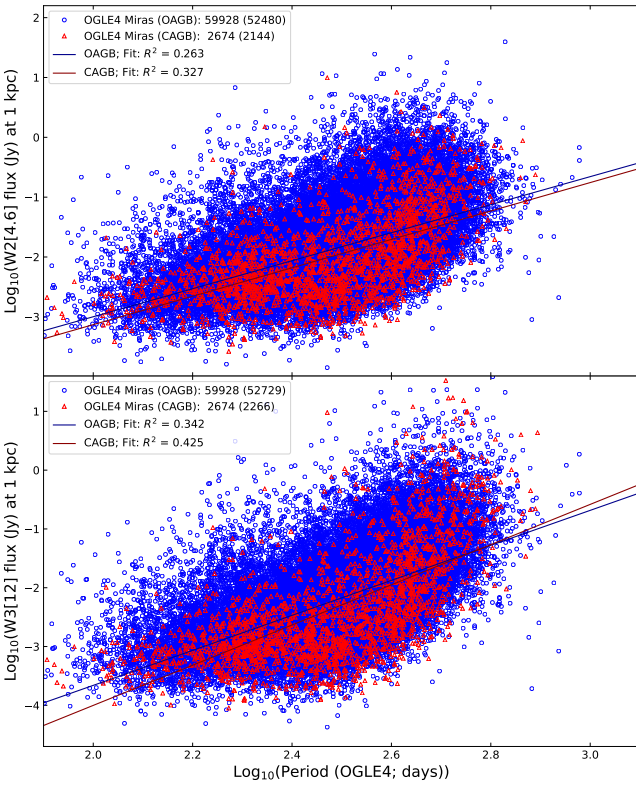


Figure 3. Period-Magnitude relations for the OGLE4 Mira variables from Iwanek et al. (2022) with known distances from Gaia DR3 (see Section 2.6).

objects (MSXC6). AKARI (Murakami et al. 2007) provided the PSC data at two bands (9 and 18 μm ; Ishihara et al. 2010) for 870,973 objects and bright-source catalogue (BSC) data at four bands (65, 90, 140, and 160 μm ; Yamamura et al. 2010) for 427,071 objects. The field of view (FOV) pixel sizes of the IRAS, MSX, AKARI PSC, and AKARI BSC images are $0'.75 \times (4'.5-4'.6)$, $18''.3$, $10''$, and $30''$, respectively.

Two-Micron All-Sky Survey (2MASS) (Cutri et al. 2003) provided PSC data at J (1.25 μm), H (1.65 μm),

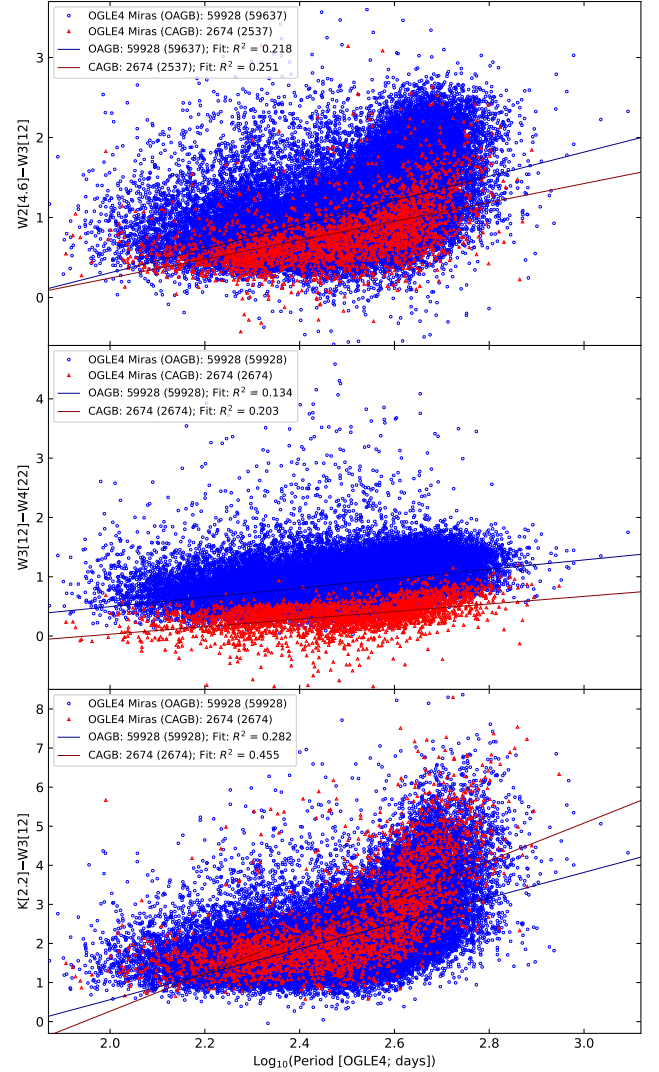


Figure 4. Period-color relations for the OGLE4 Mira variables from Iwanek et al. (2022).

and K (2.16 μm) bands for more than 470 million objects. The FOV pixel size of the 2MASS image is $2''$. WISE (Wright et al. 2010) conducted the entire sky survey at W1 (3.4 μm), W2 (4.6 μm), W3 (12 μm), and W4 (22 μm) bands. For the four WISE bands, the FOV pixel sizes are $2''.75$, $2''.75$, $2''.75$, and $5''.5$, and the 5σ photometric sensitivities are 0.068, 0.098, 0.86, and 5.4 mJy. In 2013, the AllWISE source catalog released to present more accurate positions and four-band fluxes for over 747 million objects.

The FOV pixel size of the CCD camera system for OGLE4 is $0''.26$ (see <https://ogle.astrouw.edu.pl/>).

2.2. Cross-matches

Table 1 lists the numbers of the cross-identified AllWISE, 2MASS, Gaia, and IRAS PSC counterparts for the 65,981 OGLE4 Mira variables in our Galaxy (Iwanek et al. 2022). For each object, we find the nearest cross-matched source within $5''$ ($2''$ for Gaia). See Section 2.7 for the IRAS counterparts.

In some cases, multiple OGLE4 objects may have the same cross-matched source because the telescope for OGLE4 has a smaller FOV pixel size. So we have checked all of the duplicated cross-matches and selected only the nearest object for the one source in the All-WISE, 2MASS, Gaia, and IRAS PSC. We find that there are 64,962 OGLE4 Mira variables that have All-WISE counterparts.

We need to confirm that the cross-matched sources show the expected properties (brightness, colors, etc) of the original object. A diagram comparing the fluxes of the identified source and original source is useful. In most cases, they show a good correlation (e.g., see Figure 1 in Suh 2021), but some objects show large deviations. A reason for the deviations could be because they are different objects. In this work, we have reduced the number of the deviated objects by using the multiple cross-match and comparison processes (See Section 2.7). Because another reason for the deviations could be the large scale variations of AGB stars or different beam sizes of the two telescope systems, we do not exclude the remaining objects that show the large deviations.

IR 2CDs that show a general character of the object is also useful. For OGLE4 Mira variables, the IR 2CDs using the cross-matched sources need to show that the new objects produce expected colors similar to previously known Mira variables or AGB stars (Section 2.4).

In this paper, we use only good-quality observational data for all wavelength bands for the IRAS, 2MASS, WISE, AKARI, and MSX photometric data ($q = 3$ for IRAS and AKARI; $q = A$ for 2MASS; $q = A$ or B for WISE; $q = 3$ or 4 for MSX).

2.3. Color indices

The color index is defined by

$$M_{\lambda 1} - M_{\lambda 2} = -2.5 \log_{10} \frac{F_{\lambda 1}/ZMF_{\lambda 1}}{F_{\lambda 2}/ZMF_{\lambda 2}} \quad (1)$$

where $ZMF_{\lambda i}$ is the zero magnitude flux (ZMF) at given wavelength (λi). $ZMF_{\lambda i}$ is specified in the manual for the corresponding telescope system (see Table 4 in Suh 2021).

Figures 1, 4, and 5 show IR 2CDs using various IR color indices. Note that we use only good quality observational data for all wavelength bands in plotting the IR 2CDs (see Section 2.2).

To consider the Galactic extinction processes, we plot reddening vectors for IR 2CD using NIR data (see Suh 2021 for details of the reddening vectors).

2.4. The 2MASS-WISE 2CD

IR 2CDs have been useful to distinguish different characteristics of various heavenly bodies (e.g., van der Veen & Habing 1988; Suh 2018). Though the classification using the IR spectra would be much more reliable, the IR color-selection method is useful because the method can make right classification for a major portion of

known OAGB or CAGB stars with IR spectroscopic data (Suh & Hong 2017; Suh 2021). Therefore, the IR color-selection method using an IR 2CD can be useful to distinguish between OAGB and CAGB for AGB stars without reliable spectroscopic data.

The WISE-2MASS 2CD using $W3[12]-W4[22]$ versus $K[2.2]-W3[12]$ looks to be more useful than any other 2CDs because the color-combination can distinguish different classes of AGB stars more correctly (Suh 2018; Suh 2020; Suh 2021; see Section 3.1) and the good quality observed data (for the two IR colors) are available for a larger number of sample objects. The brown line on the upper panel of Figure 1 shows the boundary line between OAGB and CAGB stars obtained for known AGB stars (Suh 2021), which is used for the color-selection method in this paper.

The upper panel of Figure 1 shows the WISE-2MASS 2CD for the OGLE4 Mira variables (see Table 1) as well as the AGB stars in the catalog of Suh (2021) (see Table 3). On this 2CD, we can find new color-selected AGB stars from the 65,981 OGLE4 Mira variables: 59,928 OAGB and 2674 CAGB stars. Because another 3379 objects do not have the good-quality observed color indices for the 2CD, the objects can not be classified using the color-selection method.

2.5. Gaia RP spectra

The Gaia DR3 LPV (Lebzelter et al. 2022) data provide the low-resolution RP spectra at visual wavelength bands to identify C-rich stars. Using the Gaia RP spectral data for the cross-identified 57,482 OGLE4 Mira variables (see Table 1), they can be classified into 56,596 O-rich and 886 C-rich stars by using the selection criteria ($7 < \text{median_delta_wl_rp} < 11$ and $G_{BP} < 19$ mag) presented in Section 2.4 in Lebzelter et al. (2022). The lower panel of Figure 1 shows the WISE-2MASS 2CD for OAGB and CAGB stars classified from the Gaia RP spectra for the OGLE4 Mira variables.

Figure 2 shows number density distributions of the Gaia magnitudes at the BP band for OAGB and CAGB stars classified from the Gaia RP spectra for the OGLE4 Mira variables. The number density in the histogram denotes the raw count divided by the total number of counts and the bin width, so that the area under the histogram integrates to one. We find that most CAGB stars classified from the Gaia RP spectra are bright nearby AGB stars.

We find that the classification using the Gaia RP spectra is right for a portion of known AGB stars with IR spectroscopic data. Compared with the color-selection method (see Section 2.4), we find that the accuracy ratio of the RP spectral method is lower (see Section 3.1). This could be due to severe interstellar extinction processes at the visual bands or the effect of dust envelopes around AGB stars. The RP spectral data would be more useful for studying nearby AGB stars with thin dust envelopes.

In this work, we do not use the Gaia RP spectral data for classifying the OGLE4 Mira variables because we believe that the color-selection method (see Section

2.4) is more useful for the large sample of AGB stars in our Galaxy. However, the catalog data for all of the sample AGB stars (see Section 3) will include the information from the available Gaia RP spectral data.

2.6. Period-magnitude and period-color relations

Figure 3 shows period-magnitude relations at W2[4.6] and W3[12] bands for the OGLE4 Mira variables from Iwanek et al. (2022) with known distances from Gaia DR3. For each object, the absolute magnitudes at the two WISE bands are calculated from the corrected distances from Bailer-Jones et al. (2021) for the cross-matched Gaia DR3 LPV object (Lebzelter et al. 2022). Generally, we find that Mira variables with longer periods show brighter IR fluxes. The large deviations from the linear relations would be mainly due to uncertainty in the Gaia distances. As expected for Mira variables (e.g., Soszyński et al. 2013; Suh 2020), we find that the OGLE4 Mira variables occupy a single sequence on the period-magnitude diagrams.

Figure 4 shows period-color relations for 59,928 OAGB and 2674 CAGB stars classified from the 65,981 OGLE4 Mira variables (see Section 2.4). Generally, we find that Mira variables with longer periods show redder IR colors. Mira variables with longer periods are expected to have thicker dust envelopes as they are generally more evolved AGB stars.

2.7. IRAS PSC sources

Because IRAS has very low angular resolution, the AllWISE or 2MASS counterparts obtained from the positions of cross-matched AKARI or MSX sources (with a higher angular resolution; see Section 2.1) would be much more reliable.

For all of the 245,889 IRAS PSC sources, we have found the AKARI, MSX, AllWISE, 2MASS, OGLE4, Gaia DR3, and AAVSO counterparts by using following method. We cross-identify the AKARI PSC, MSX, and AKARI BSC counterpart by finding the nearest source within $60''$ using the position given in the IRAS PSC (version 2.1). Then, we cross-identify the AllWISE, 2MASS, and OGLE4 counterparts using the best position of the available AKARI PSC, MSX, or AKARI BSC counterpart. Only when there is no AKARI or MSX counterpart, we use the position of the IRAS PSC.

The similar method was used in Suh (2018) and Suh (2021). But in this work, we use the MSX data in addition to the AKARI data to improve the accuracy of the cross-match (see Section 2.2).

From the 65,981 OGLE4 Mira variables, we find 18,413 IRAS counterparts (excluding duplicate sources) within $60''$. From the 18,426 sources, we find that 16,379 sources are positive (or reliable) counterparts, for which the AllWISE counterpart of the IRAS source is the same as the AllWISE counterpart of the OGLE4M object (see Table 2).

3. A NEW SAMPLE OF AGB STARS

Suh (2021) presented a catalog AGB stars in our Galaxy in two parts: one is based on the IRAS PSC and the

other one is based on the AllWISE source catalog. In the IRAS based catalog, there are 5908 OAGB-IRAS and 3596 CAGB-IRAS objects. And in the AllWISE based catalog, there are 5301 OAGB-WISE and 3576 CAGB-WISE objects. Because IRAS has lower angular resolution and weaker sensitivity (see Section 2.1) than WISE, the AGB-IRAS objects are generally brighter than the AGB-IRAS objects.

In this work, we revise and update the catalog using the new sample of OGLE4 Mira variables presented by Iwanek et al. (2022). We use the color-selection method (see Section 2.4) to classify the OGLE4 Mira variables into OAGB or CAGB stars, except for the objects for which more reliable IR spectroscopic data are available.

We present a new catalog of 19,196 OAGB-IRAS, 4118 CAGB-IRAS, 45,413 OAGB-WISE, and 5366 CAGB-WISE objects (see Tables 3 and 4). For the new list of AGB stars, we cross-identify the IRAS, AKARI, MSX, AllWISE, 2MASS, OGLE4, Gaia DR3, and AAVSO counterparts and present the new catalog data, which contain all of the available information.

Among the 65,981 OGLE4 Mira variables from Iwanek et al. (2022), 62,989 objects (15,248 OAGB-IRAS, 797 CAGB-IRAS, 44,977 OAGB-WISE, and 1967 CAGB-WISE) are included in the new catalog of OAGB and CAGB stars and 2000 objects are classified into NI-O4 or NW-O4 subgroups (see Tables 3 and 4). And 992 objects are not included in the catalog because 984 objects do not have the AllWISE counterparts and can not be cross-identified as any known AGB stars and another 8 objects can be cross-identified as known S type or silicate-carbon stars.

3.1. AGB stars based on the IRAS PSC

Suh (2021) presented a catalog AGB stars in our Galaxy that is based on the IRAS PSC: 5908 OAGB-IRAS and 3596 CAGB-IRAS objects. We revise and update the catalog using the new sample of OGLE4 Mira variables presented by Iwanek et al. (2022).

In identifying important dust features of AGB stars, IRAS Low Resolution Spectrograph (LRS; $\lambda = 8\text{--}22\text{ }\mu\text{m}$) data are useful (Kwok et al. 1997). For OAGB stars, the IRAS LRS class E objects show the $10\text{ }\mu\text{m}$ silicate feature in emission and class A objects show the $10\text{ }\mu\text{m}$ silicate feature in absorption. For CAGB stars, the LRS class C objects show the $11.3\text{ }\mu\text{m}$ SiC feature in emission.

For CAGB stars in the IRAS LRS class C, the accuracy ratio of the color-selection method (see Section 2.4) is 82 %, while the accuracy ratio of the Gaia RP spectral method (see Section 2.5) is 55 %. For OAGB stars in the IRAS LRS class E or A, the inaccuracy ratios of the two methods are about the same.

Table 3 lists a new catalog of AGB-IRAS objects. We correct some misidentified objects from Suh (2021). We add the OGLE4 Mira variables (presented by Iwanek et al. 2022) with the positive IRAS counterparts (see Section 2.7), which are classified into OAGB

Table 2
IRAS PSC sources

IRAS PSC ¹	AKARI PSC ²	MSX ²	AKARI BSC ²	AllWISE ³	2MASS ³	OGLE4M ^{3,4}	Gaia ^{3,5}
245,889	159,031	82,001	61,705	245,756	245,049	16,379	98,522

¹version 2.1. ²The number of counterparts within 60'' using the IRAS position (duplicate sources are excluded). ³The number of counterparts within 60'' using the best position from IRAS, AKARI, and MSX (duplicate sources are excluded). ⁴The number of positive counterparts within 60'' (see Section 2.7). ⁵Gaia DR3 LPV object (Lebzelter et al. 2022).

Table 3
Sample of AGB stars based on the IRAS PSC (AGB-IRAS)

Class	Subgroup	Reference	Number	Selected	Duplicate	AE ¹	Remaining
OAGB-IRAS	OAGB-IRAS(2021)	Suh (2021)	5908	5908	0	-1 ²	5907
OAGB-IRAS	OI-O4S	This work	16,379 ³	2273 ⁴	646 ⁵	0	1627
OAGB-IRAS	OI-O4C	This work	16,379 ³	12,920 ⁶	1258 ⁵	0	11,662
OAGB-IRAS	OAGB-IRAS(2022)	Total	-	-	-	-	19,196
CAGB-IRAS	CAGB-IRAS(2021)	Suh (2021)	3596	3596	0	-1 ⁷	3595
CAGB-IRAS	CI-O4S	This work	16,379 ³	295 ⁸	243 ⁹	0	52
CAGB-IRAS	CI-O4C	This work	16,379 ³	493 ⁶	22 ¹⁰	0	471
CAGB-IRAS	CAGB-IRAS(2022)	Total	-	-	-	-	4118
No class	NI-O4	This work	16,379 ³	398 ⁶	37 ⁵	-	361

¹added or excluded. ²IRAS 17056-3959 is a carbon star (now in CI-O4S). ³the number (16379) of positive IRAS counterparts from all of the OGLE4 Mira variables (see Section 2.7). ⁴objects with O-rich spectra from IRAS LRS and/or SIMBAD. ⁵in OAGB-IRAS(2021) or CAGB-IRAS(2021) or in the list of S stars or silicate-carbon stars in AGB-IRAS (Suh 2021). ⁶color-selected OAGB, CAGB, or No class objects (see Section 2.4). ⁷IRAS 17514-3354 is an OAGB star (now in OI-O4C). ⁸objects with C-rich spectra from SIMBAD. ⁹in CI-2021. ¹⁰in CI-2021 or OI-2021.

Table 4
Sample of AGB stars based on the AllWISE source catalog (AGB-WISE)

Class	Subgroup	Reference	Number	Selected	Duplicate	Remaining
OAGB-WISE	OAGB-WISE(2021)	Suh (2021)	5301	5301	4 ¹ +49 ²	5248
OAGB-WISE	OW-O4C	This work	64,962 ³	59,928 ⁴	14,936 ⁵ +4827 ⁶	40,165
OAGB-WISE	OAGB-WISE(2022)	Total	-	-	-	45,413
CAGB-WISE	CAGB-WISE(2021)	Suh (2021)	3576	3576	2 ⁷ +2 ⁸	3572
CAGB-WISE	CW-O4C	This work	64,962 ³	2674 ⁴	728 ⁹ +152 ⁶	1794
CAGB-WISE	CAGB-WISE(2022)	Total	-	-	-	5366
No class	NW-O4	This work	64,962 ³	2360 ⁴	715 ¹⁰ +6 ⁶	1639

¹in OAGB-IRAS(2021). ²in OI-O4S or OI-O4C. ³the number of OGLE4 Mira variables with AllWISE counterparts (see Table 1). ⁴color-selected OAGB, CAGB, or No class objects (see Section 2.4). ⁵in OI-O4S, OI-O4C, or CI-O4S. ⁶in OAGB-WISE(2021) or CAGB-WISE(2021). ⁷in CAGB-IRAS(2021) or OAGB-IRAS(2021). ⁸in CI-O4S or CI-O4C. ⁹in CI-O4S, CI-O4C, or OI-O4S. ¹⁰in NI-O4.

and CAGB stars using the color-selection method using the WISE-2MASS 2CD (see Section 2.4).

In classifying into OAGB or CAGB, the more reliable method using the spectral information (the spectral type from the IRAS LRS or SIMBAD) gets priority over the color-selection method using IR 2CDs.

Finally, we present a new list of 23,314 AGB-IRAS objects, which are classified into 19,196 OAGB-IRAS and 4118 CAGB-IRAS stars.

3.2. AGB stars based on the AllWISE source catalog

Suh (2021) presented a catalog AGB stars in our Galaxy that is based on the AllWISE source catalog: 5301 OAGB-WISE and 3576 CAGB-WISE objects. We revise and update the catalog using the new sample of OGLE4 Mira variables presented by Iwanek et al. (2022).

Table 4 lists a new catalog of AGB-WISE objects. They are identified based on the AllWISE source catalog and do not have positive IRAS counterparts. We make corrections for some misidentified AGB-WISE objects from Suh (2021). We add the OGLE4 Mira variables (presented by Iwanek et al. 2022) with the AllWISE counterparts.

Now, we present a new list of 50,779 AGB-WISE objects, which are classified into 45,413 OAGB-WISE and 5366 CAGB-WISE stars.

4. IR 2CDs AND DISCUSSION

Figures 5 and 6 show various 2CDs for AGB stars in the new revised and extended catalog (see Section 3; Tables 3 and 4). On all of the 2CDs in Figures 1, 5, and 6, theoretical models for AGB stars are also plotted to be compared with the observations.

4.1. Theoretical Dust Shell Models

In this paper, we use the same theoretical dust shell models as the ones used in Suh (2020) and Suh (2021) (see Section 3 and Table 7 in Suh (2021) for the summary). We use the radiative transfer code DUSTY (Ivezić & Elitzur 1997), which assumes a spherically symmetric dust shell around a central star. We assume that the central stars is a black body ($T = 3000\text{--}2000$ K).

For all models, we use a simple power law ($\rho \propto r^{-2}$) for the dust density distribution and assume that the dust formation temperature (T_c) is 1000–500 K. The outer radius of the dust shell is taken to be 10^4 times the inner radius, the fiducial wavelength of the dust shell optical depth (τ_{10}) is $10 \mu\text{m}$, and the uniform radius of spherical dust grains is $0.1 \mu\text{m}$.

For OAGB stars, we use dust optical constants of warm and cold silicates (Suh 1999), amorphous alumina (Suh 2016), and $\text{Fe}_{0.9}\text{Mg}_{0.1}\text{O}$ (Henning et al. 1995). For CAGB stars, we use dust optical constants of AMC (Suh 2000), SiC (Pégourié 1988), and $\text{Mg}_{0.9}\text{Fe}_{0.1}\text{S}$ (Begemann et al. 1994).

On the 2CDs in Figures 1, 4, and 5, theoretical models for AGB stars are plotted. For OAGB models (silicate $T_c = 1000$ K), the model results for $\tau_{10} =$

0.001, 0.01, 0.05, 0.1, 0.5, 1, 3, 7, 15, 30, and 40 are plotted from left to right on the 2CDs. For CAGB models (AMC $T_c = 1000$ K), the model results for $\tau_{10} = 0.001, 0.01, 0.1, 0.5, 1, 2, 3,$ and 5 are plotted from left to right on the 2CDs.

For physical implications of the theoretical dust shell models, refer to Suh (2020) and Suh (2021). Suh (2020) investigated IR properties of AGB Stars in Our Galaxy and the Magellanic Clouds and discussed the physical implications (e.g., mass-loss rates, masses, ages, and metallicities) of the theoretical model parameters for different classes of AGB stars. Those model parameters were obtained from the comparison of the theoretical dust shell models with the observations on various IR 2CDs.

4.2. Comparison between Theory and Observations

On various IR 2CDs in Figures 5 and 6, we compare the observations with the theoretical dust shell models for AGB stars. Generally, the theoretical dust shell models for OAGB and CAGB stars can reproduce the observed points fairly well.

The upper panel of Figure 5 plots an IRAS 2CD using $[25]\text{--}[60]$ versus $[12]\text{--}[25]$. A group of CAGB stars in the upper-left region are visual carbon stars that show excessive flux at $60 \mu\text{m}$ due to the remnant of the earlier phase when they were OAGB stars (e.g. Chan & Kwok 1990). Another group of CAGB stars in the lower region, which extends to the right side, are IR carbon stars. The IR carbon stars with redder $[12]\text{--}[25]$ colors are believed to be more evolved or massive stars with thicker dust envelope (see Section 1 in Suh 2020 for origin and evolution of carbon stars).

The lower panel of Figure 5 plots an 2MASS-IRAS 2CD using $\text{IR}[12]\text{--}\text{IR}[60]$ versus $\text{K}[2.2]\text{--}\text{IR}[12]$. On this 2CD, the distinguishment between OAGB and CAGB stars is clearer. Visual carbon stars are located in the lower-left region on this 2CD, because they show bluer $\text{K}[2.2]\text{--}\text{IR}[12]$ and $\text{IR}[12]\text{--}\text{IR}[60]$ colors than IR carbon stars.

Figure 6 shows 2CDs using WISE and 2MASS colors. The upper panel of Figure 6 shows a WISE 2CDs using $\text{W3}[12]\text{--}\text{W4}[22]$ versus $\text{W2}[4.6]\text{--}\text{W3}[12]$. The lower panel of Figure 6 shows a WISE-2MASS 2CD using $\text{W3}[12]\text{--}\text{W4}[22]$ versus $\text{K}[2.2]\text{--}\text{W3}[12]$. On these 2CDs, the theoretical dust shell models for CAGB stars with various C-rich dust grains can reproduce a wider range of observed $\text{W3}[12]\text{--}\text{W4}[22]$ colors.

In the lower regions of the 2CDs in Figure 6, we find that there are many newly identified CAGB-IRAS or CAGB-WISE objects in this work, which are color-selected from the OGLE4 Mira variables (see Section 2.4). We may need to confirm the C-rich nature of these objects by using a more reliable IR spectroscopic method. The objects in the upper-left regions on the 2CDs in Figure 6 are likely to be early stage OAGB stars or visual carbon stars with thin and detached dust shells ($T_c = 200\text{--}300$ K; see Suh 2020).

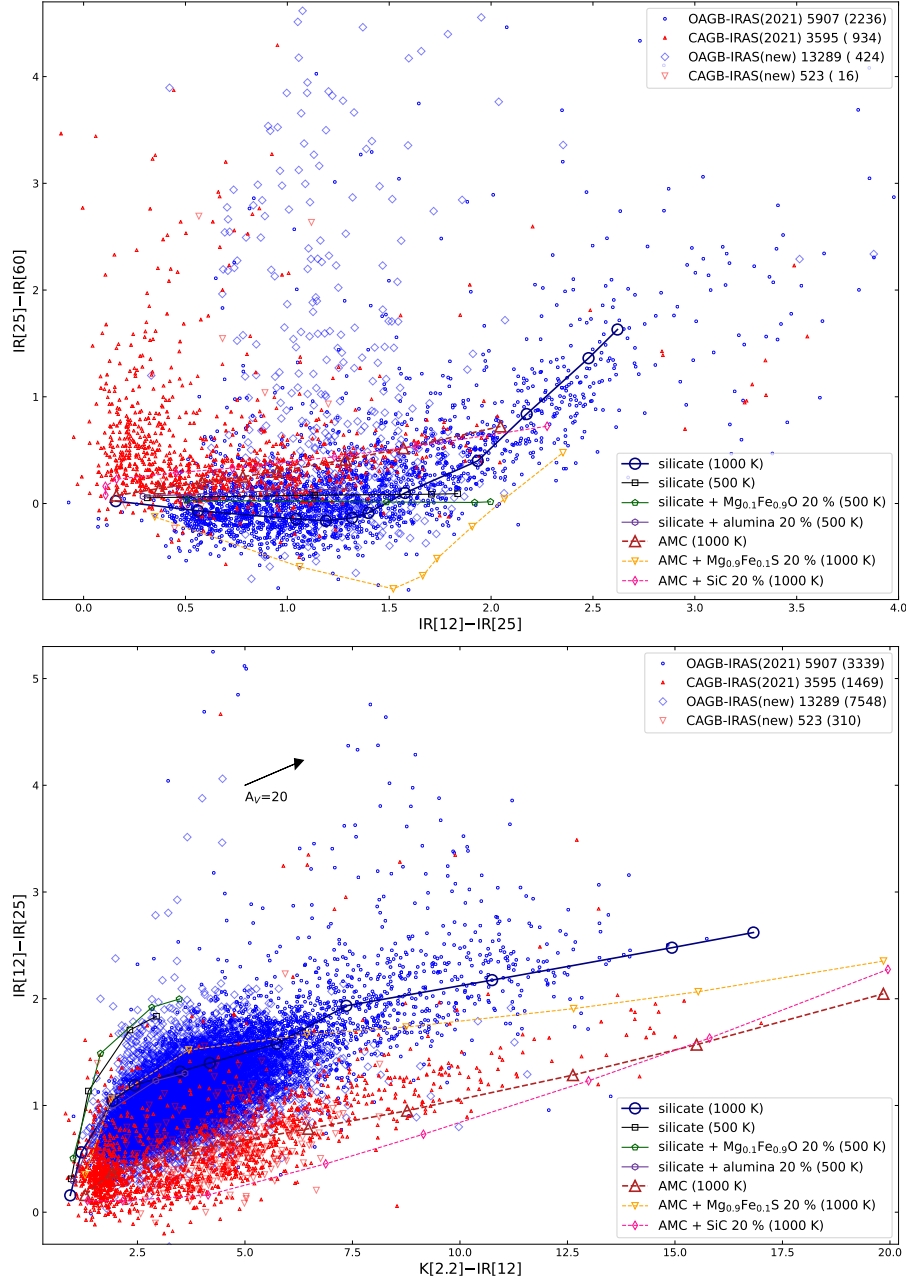


Figure 5. IRAS-2MASS 2CDs for AGB-IRAS stars in the previous catalog of [Suh \(2021\)](#) and new AGB-IRAS stars identified from the OGLE4 Mira variables (see [Tables 3](#)) compared with theoretical models (see [Section 4.1](#)). The number of objects and the number of plotted objects (in parenthesis) with good-quality observed data are shown for each class.

4.3. Statistical properties of AGB stars

Figure 7 shows the error bar plots of the observed colors on the various 2CDs used for all classes of AGB stars presented in [Figures 5 and 6](#). Because IRAS LRS class A objects (mostly OH/IR stars) and class C objects (IR carbon stars) have thicker dust envelopes, they are believed to be more evolved or massive AGB stars. We find that these more evolved OAGB or CAGB objects with thicker dust envelopes show redder colors for all of the IR color indices except for the [25]–[60] color. This is because visual carbon stars with thin dust envelopes show excessive flux at 60 μ m. Gener-

ally, AGB-WISE objects show bluer colors compared with AGB-IRAS objects. This would be because most AGB-WISE objects are less evolved and have thinner dust shells than AGB-IRAS objects.

Figure 8 shows number density distributions of $K[2.2]$ – $W3[12]$ indices for AGB-IRAS and AGB-WISE stars. Compared with AGB-WISE objects, more AGB-IRAS objects show redder colors because they have thicker dust envelopes. Compared with CAGB-IRAS objects, OAGB-IRAS objects show redder colors.

Figure 9 shows number density distributions of the OGLE4 periods for AGB-IRAS and AGB-WISE stars.

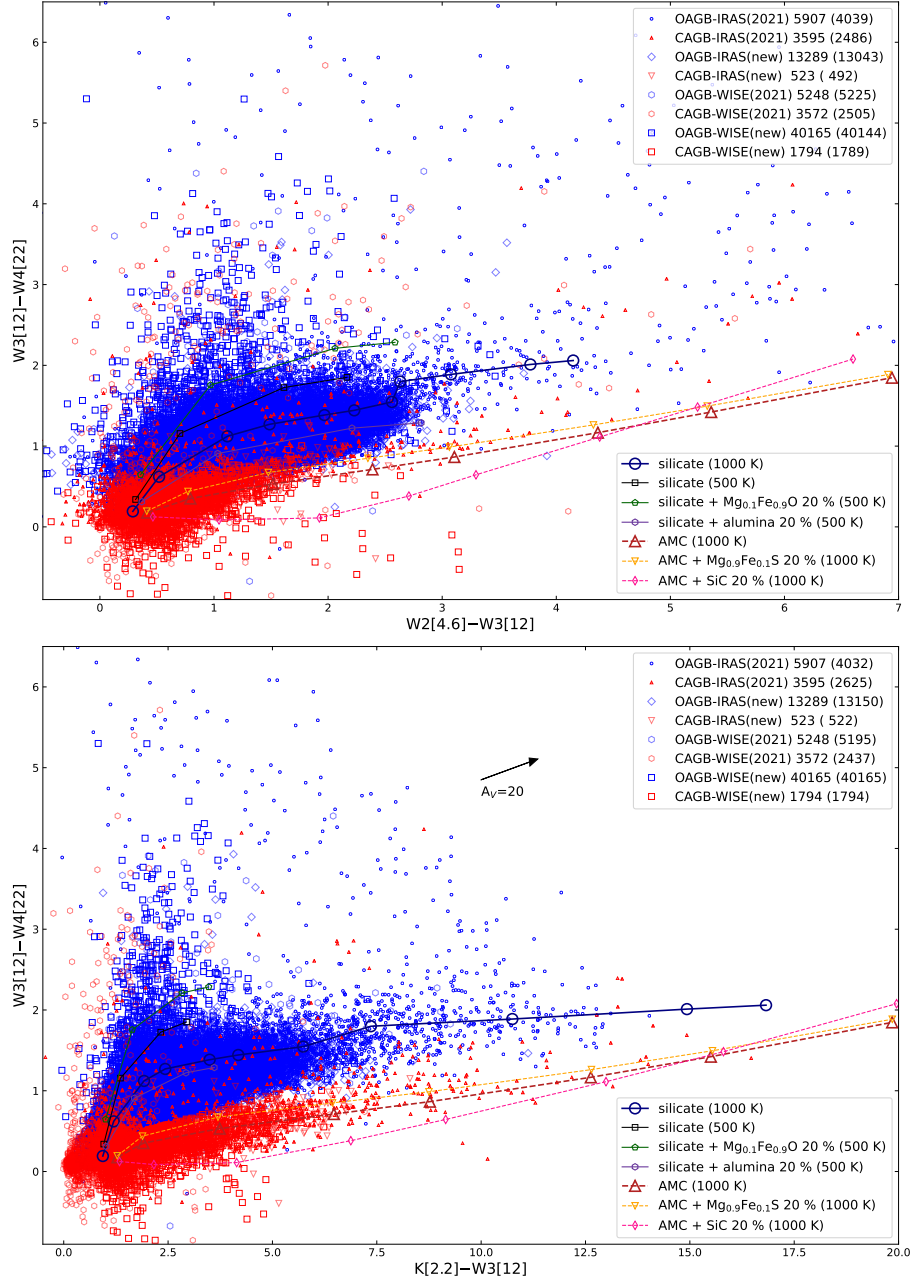


Figure 6. WISE-2MASS 2CDs for all AGB stars in the previous catalog of [Suh \(2021\)](#) and new AGB stars identified from the OGLE4 Mira variables (see Tables 3 and 4) compared with theoretical models (see Section 4.1). The number of objects and the number of plotted objects (in parenthesis) with good-quality observed data are shown for each class.

We find that more AGB-IRAS objects show longer averaged pulsation periods than AGB-WISE objects, which are generally less evolved or less massive. We also find that CAGB-IRAS stars show generally longer periods than OAGB-IRAS stars. This would be due to a selection effect of OGLE4 observations. Because the OGLE4 periods are obtained from the I filter photometry, most OAGB-IRAS stars with thick dust envelopes and longer pulsation periods (OH/IR stars) are not observed by the OGLE4 observations.

5. SUMMARY

We have investigated infrared properties of OGLE4 Mira variables in our Galaxy. For each object, we have cross-identified the AllWISE, 2MASS, and IRAS counterparts. We have presented various infrared two-color diagrams (2CDs) and period-magnitude and period-color relations for the Mira variables. Generally, the Mira variables with longer periods are brighter in the IR fluxes and redder in IR colors.

We have revised and updated the catalog of AGB stars in our Galaxy from [Suh \(2021\)](#) using the new sample of OGLE4 Mira variables. Now, we present a new

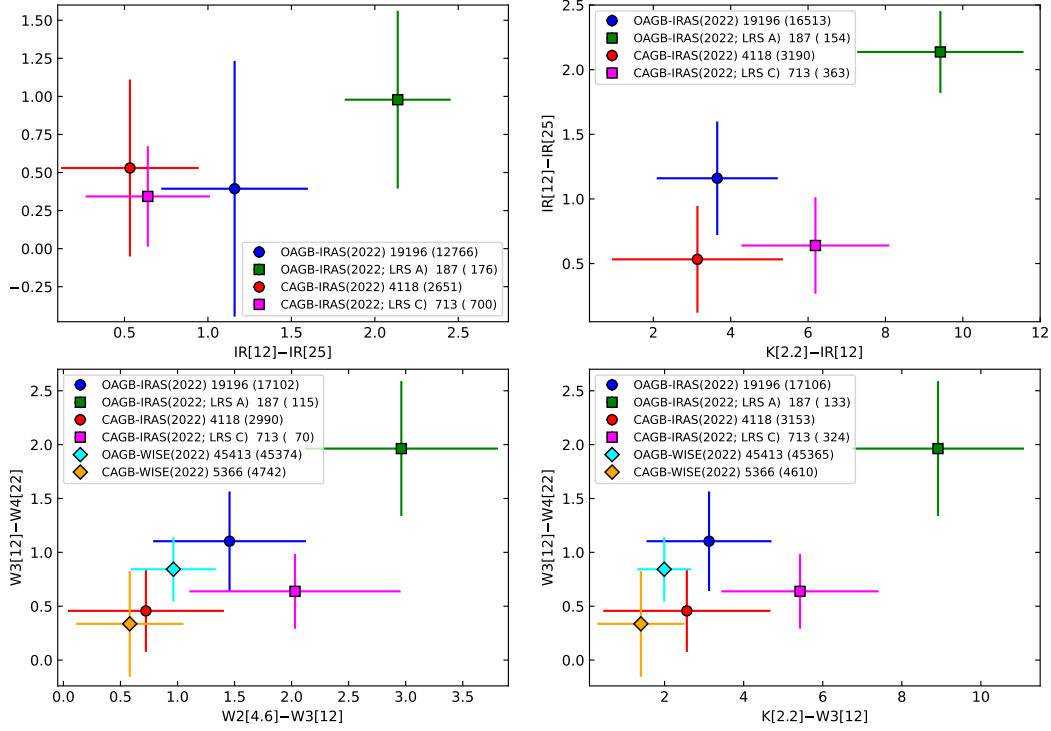


Figure 7. Averaged observed IR colors for different classes of AGB stars (see Tables 3 and 4; Figures 4 and 5). The number of objects and the number of considered objects (in parenthesis) with good-quality observed data for the horizontal axis are shown for each class.

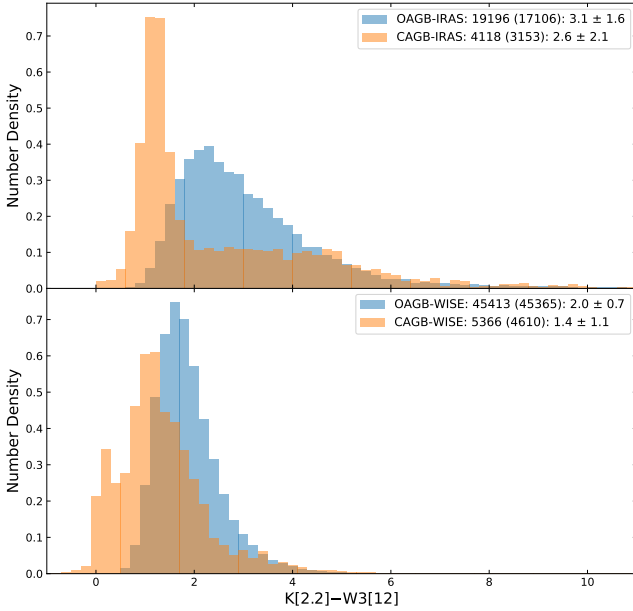


Figure 8. Number density distributions of observed $K[2.2]-W3[12]$ indices for AGB-IRAS and AGB-WISE stars. The number of objects and the number of considered objects (in parenthesis) with good-quality observed data are shown for each class.

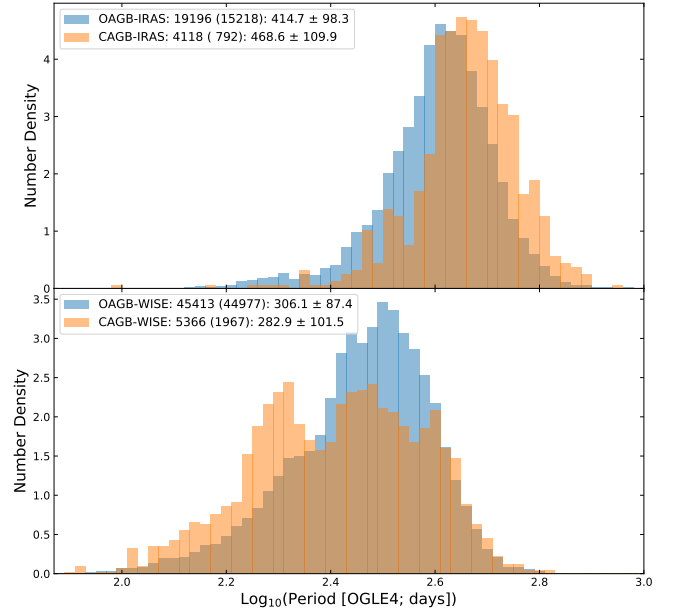


Figure 9. Number density distributions of the observed OGLE4 periods for AGB-IRAS and AGB-WISE stars.

catalog of 74,093 (64,609 OAGB and 9484 CAGB) stars in our Galaxy. A group of 23,314 (19,196 OAGB-IRAS and 4118 CAGB-IRAS) stars are identified based on the

IRAS PSC and another group of 50,779 (45,413 OAGB-WISE and 5366 CAGB-WISE) stars are identified based on the AllWISE source catalog.

For all of the AGB stars in the new catalog, we have cross-identified the IRAS, AKARI, MSX, AllWISE, 2MASS, OGLE4, Gaia DR3, and AAVSO counterparts

and presented a new catalog data, which contains all of the available information.

We have presented various IR 2CDs for all AGB stars in the catalog. Comparing the observations with the theory on the 2CDs, we have found that basic theoretical dust shell models can account for the IR observations fairly well for most of the AGB stars.

We have found that the AGB-IRAS objects show longer averaged pulsation periods and redder averaged IR colors than AGB-WISE objects, which are generally less evolved or less massive.

The new revised and updated data for the catalog of AGB stars in our Galaxy (version 2022) will be accessible through the author's webpage (<https://web.chungbuk.ac.kr/~kwsuh/agb.htm>).

ACKNOWLEDGMENTS

This research was supported by Basic Science Research Program through the National Research Foundation of Korea (NRF) funded by the Ministry of Education (2022R1I1A3055131). This research has made use of the VizieR catalogue access tool and the SIMBAD database, operated at CDS, Strasbourg, France. This research has made use of the NASA/IPAC Infrared Science Archive, which is operated by the Jet Propulsion Laboratory, California Institute of Technology, under contract with the National Aeronautics and Space Administration.

REFERENCES

- Bailer-Jones, C., Rybizki, J., Fousneau, M., et al. 2021, Estimating Distances from Parallaxes. V. Geometric and Photogeometric Distances to 1.47 Billion Stars in Gaia Early Data Release 3, *AJ*, 161, 147
- Begemann, B., Dorschner, J., Henning, T., Mutschke, H., & Thamm, E. 1994, A Laboratory Approach to the Interstellar Sulfide Dust Problem, *ApJ*, 423, L71
- Begemann, B., Dorschner, J., Henning, T., et al. 1997, Aluminum Oxide and the Opacity of Oxygen-Rich Circumstellar Dust in the 12-17 Micron Range, *ApJ*, 476, 199
- Beichman, C. A., Neugebauer, G., Habing, H., Clegg, P. E., & Chester, T. C. 1988, IRAS Catalogs and Atlases: Explanatory Supplement, NASA RP-1190 (Washington: NASA)
- Chan, S. J., & Kwok, S., 1990, Evolution of Infrared Carbon Stars, *A&A*, 237, 354
- Cutri, R. M., Skrutskie, M. F., Van Dyk, S., et al. 2003, VizieR Online Data Catalog: 2MASS All-Sky Catalog of Point Sources
- Egan, M. P., Price, S. D., & Kraemer, K. E. 2003, The Mid-course Space Experiment Point Source Catalog v2.3 (2003 October) Air Force Research Lab. Tech. Rep. AFRL-VS-TR-2003-1589 (Springfield, VA: NTIS)
- Henning, T., Begemann, B., Mutschke, H., & Dorschner, J. 1995, Optical Properties Of Oxide Dust Grains, *A&AS*, 112, 143
- Höfner, S., & Olofsson, H., 2018, Mass loss of stars on the asymptotic giant branch: Mechanisms, models and measurements, *A&A Rev.*, 26, 1
- Ishihara, D., Acke, B., Verhoelst, T., et al. 2010, The AKARI/IRC Mid-Infrared All-Sky Survey, *A&A*, 514, A1
- Iwanek, P., Soszyński, I., Kozłowski, S. et al. 2022, The OGLE Collection of Variable Stars: Nearly 66,000 Mira Stars in the Milky Way, *ApJS*, 260, 46
- Ivezić, A., & Elitzur, M. 1997, Self-Similarity and Scaling Behaviour of Infrared Emission from Radiatively Heated Dust - I. Theory, *MNRAS*, 287, 799
- Kwok, S., Volk, K., & Bidelman, W. P. 1997, Classification and Identification of IRAS Sources with Low-Resolution Spectra, *ApJS*, 112, 557
- Lebzelter, T., Mowlavi, N., Lecoœur-Taibi, I., et al. 2022, Gaia Data Release 3: The second Gaia catalogue of Long-Period Variable candidates, *A&A*, in press
- Murakami, H., Baba, H., Barthel, P., et al. 2007, The Infrared Astronomical Mission AKARI, *PASJ*, 59, 369
- Pégourié, B. 1988, Optical Properties of Alpha Silicon Carbide, *A&A*, 194, 335
- Soszyński, I., Wood, P. R., Udalski, A. 2013, *ApJ*, 779, 167
- Suh, K.-W. 1999, Optical Properties of the Silicate Dust Grains in the Envelopes around Asymptotic Giant Branch Stars, *MNRAS*, 304, 389
- Suh, K.-W. 2000, Optical Properties of the Carbon Dust Grains in the Envelopes around Asymptotic Giant Branch Stars, *MNRAS*, 315, 740
- Suh, K.-W. 2015, Infrared Two-Color Diagrams for AGB Stars, Post-AGB Stars, and Planetary Nebulae, *ApJ*, 808, 165
- Suh, K.-W. 2016, Optical Properties of Amorphous Alumina Dust in the Envelopes Around O-Rich AGB Stars, *JKAS*, 49, 127
- Suh, K.-W. 2018, Infrared Two-Color Diagrams of AGB stars and Planetary Nebulae using WISE data, *JKAS*, 51, 155
- Suh, K.-W. 2020, Infrared Properties of Asymptotic Giant Branch Stars in Our Galaxy and the Magellanic Clouds, *ApJ*, 891, 43
- Suh, K.-W. 2021, A New Catalog of Asymptotic Giant Branch Stars in Our Galaxy, *ApJS*, 256, 43
- Suh, K.-W., & Hong, J. 2017, A New Catalog of AGB Stars Based on Infrared Two-Color Diagrams, *JKAS*, 50, 131
- van der Veen, W. E. C. J., & Habing, H. J. 1988, The IRAS Two-Colour Diagram as a Tool for Studying Late Stages of Stellar Evolution, *A&A*, 194, 125
- Watson, C., Henden, A. A., & Price, A. 2022, VizieR, *B/vsx/vsx*
- Wright, E. L., Eisenhardt, P. R. M., Mainzer, A. K., et al. 2010, The Wide-Field Infrared Survey Explorer (WISE): Mission Description And Initial On-Orbit Performance, *AJ*, 140, 1868
- Yamamura, I., Makiuti, S., Ikeda, N., et al. 2010, AKARI/FIS All-Sky Survey Bright Source Catalogue Version 1.0 Release Note